JBC Papers in Press. Published on January 18, 2019 as Manuscript RA118.004732
The latest version is at http://www.jbc.org/cgi/doi/10.1074/jbc.RA118.004732

Structural insights into the tyrosine phosphorylation-mediated inhibition of SH3 domain-ligand interactions

Balázs Merő[1,§], László Radnai[1,§,*,#], Gergő Gógl[2], Orsolya Tőke[3], Ibolya Leveles[1,4], Kitti Koprivanacz[1], Bálint Szeder[1], Metta Dülk[1], Gyöngyi Kudlik[1], Virág Vas[1], Anna Cserkaszky[1], Szabolcs Sipeki[5], László Nyitray[2], Beáta G. Vértessy[1,4], László Buday[1,5,*]

From the [1]Institute of Enzymology, RCNS, Hungarian Academy of Sciences, Magyar tudósok körútja 2., Budapest, Hungary, H-1117; [2]Department of Biochemistry, Eötvös Loránd University, Pázmány Péter sétány 1/C, Budapest, Hungary, H-1117; [3]Laboratory for NMR Spectroscopy, RCNS, Hungarian Academy of Sciences, Magyar tudósok körútja 2., Budapest, Hungary, H-1117; [4]Department of Applied Biotechnology and Food Sciences; Budapest University of Technology and Economics; Szt. Gellért tér 4., Budapest, Hungary, H-1111; [5]Department of Medical Chemistry, Semmelweis University Medical School, Tűzoltó u. 37-47., Budapest, Hungary, H-1094

Running title: *Tyrosine phosphorylation inhibits SH3 domain ligand binding*

[§]These authors contributed equally to this work
[#]Present Address: Department of Molecular Medicine, The Scripps Research Institute, 130 Scripps Way, Jupiter, FL 33458

[*]To whom correspondence should be addressed:
László Radnai: Department of Molecular Medicine, The Scripps Research Institute, 130 Scripps Way, Jupiter, FL 33458; lradnai@scripps.edu; Tel. (561) 228-2690
László Buday: Institute of Enzymology, RCNS, Hungarian Academy of Sciences, Magyar tudósok körútja 2., Budapest, Hungary, H-1117; buday.laszlo@ttk.mta.hu; Tel. +36 1 382 6700

Key words: ABL tyrosine kinase, Src homology 3 domain (SH3 domain), ligand binding, 3BP-2, protein phosphorylation, phosphotyrosine signaling, post-translational modification (PTM), X-ray crystallography, nuclear magnetic resonance (NMR), small-angle X-ray scattering (SAXS)

ABSTRACT

Src homology 3 (SH3) domains bind proline-rich linear motifs in eukaryotes. By mediating inter- and intramolecular interactions, they regulate the functions of many proteins involved in a wide variety of signal transduction pathways. Phosphorylation at different tyrosine residues in SH3 domains have been reported previously. In several cases, the functional consequences have also been investigated. However, a full understanding of the effects of tyrosine phosphorylation on the ligand interactions and cellular functions of SH3 domains requires detailed structural, atomic-resolution studies along with biochemical and biophysical analyses. Here, we present the first crystal structures of tyrosine-phosphorylated human SH3 domains derived from the Abelson-family kinases ABL1 and ABL2 at 1.6 and 1.4 Å resolutions, respectively. The structures revealed that simultaneous phosphorylation of Tyr-89 and Tyr-134 in ABL1, or the homologous residues Tyr-116 and Tyr-161 in ABL2 induce only minor structural perturbations. Instead, the phosphate groups sterically blocked the ligand-binding grooves, thereby strongly inhibiting the interaction with proline-rich peptide ligands. Although some crystal contact surfaces involving phosphotyrosines suggested the possibility of tyrosine-phosphorylation induced dimerization, we excluded this possibility by using small-angle X-ray scattering (SAXS), dynamic light scattering (DLS), and NMR relaxation analyses. Extensive analysis of relevant databases and literature revealed that the residues phosphorylated in our model systems are not only well conserved in other human SH3 domains, but that the corresponding tyrosines are known

phosphorylation sites *in vivo* in many cases. We conclude that tyrosine phosphorylation might be a mechanism involved in the regulation of the human SH3 interactome.

Src homology 3 (SH3) domains are protein-protein interaction domains in eukaryotes involved in various intracellular signaling pathways (1,2). More than 200 human proteins are known to possess one or more SH3 domains. These proteins play various roles in fundamental cellular processes, such as the regulation of cellular movement or proliferation, and are also involved in the development of cancer and several other disorders. SH3 domains are relatively small (~60 residues) and have an antiparallel β-sandwich topology that is formed by five β-strands (βa, βb, βc, βd, and βe) connected by three loops (RT, N-Src, and distal loops) and a short 3_{10} helix (Fig. 1/A) (1,2). SH3 domains usually bind short, proline-rich sequences within intrinsically unstructured regions of partner proteins. These linear motifs adopt a left-handed polyproline type II helix conformation. Some SH3 domains are also involved in intramolecular interactions. The most strictly defined consensus sequence of the SH3-binding linear motifs is PxxP, where "x" denotes any amino acid. There is usually a positively charged residue on either side of the consensus motif (+xxPxxP or xPxxPx+) (1,2). The shallow, hydrophobic ligand-binding groove bounded by the RT and the N-Src loops is mostly comprised of aromatic residues. This interface can be further divided into three smaller pockets (Pocket I-III). Pocket I and II are mainly hydrophobic and accommodate two residues of the binding motif ("Px" or "xP", where "x" is a hydrophobic residue). One or more negatively charged residue of the RT loop can often be found in Pocket III orienting the ligands through electrostatic interaction with a positively charged residue on either side of the PxxP motif (Fig. 1/A) (3).

A recent study showed that tyrosine phosphorylation occurs frequently in SH3 domains (4). Most of the involved tyrosines are part of the ligand binding groove, and the result of this post-translational modification was the inhibition of partner binding *in vivo* in the majority of reported cases (4). However, to fully understand the role and function of tyrosine phosphorylation, detailed structural studies at atomic resolution complemented by biochemical and biophysical methods assessing SH3-ligand interactions would be crucial. Therefore, we have chosen ABL1 and ABL2, two SH3-containing non-receptor tyrosine kinases belonging to the ABL family (5), as a model system to study SH3 domain tyrosine phosphorylation *in vitro*.

ABL kinases are key regulators of different signal transduction pathways in numerous cell types influencing proliferation, differentiation, survival, death, morphology, motility, and adhesions of cells (5). The SH3 domains of ABL1 and ABL2 or their constitutively active chimeric fusion protein forms (which are responsible for certain human leukemias, such as BCR-ABL (6)) were reported to be phosphorylated *in vivo* at three homologous tyrosine residues: Tyr89 (7,8) and Tyr134 (8,9) within and Tyr112 outside of the ligand binding groove in ABL1, while Tyr116 and Tyr161 (10) within and Tyr139 (10) outside of the ligand binding groove in ABL2 (Fig. 1/B). While tyrosine phosphorylation at multiple sites within the SH3-SH2 region was found to be necessary for full BCR-ABL transforming activity, substitution of Tyr89 to phenylalanine was solely sufficient to strongly reduce BCR-ABL-mediated transformation (8). Inhibition of myeloid Src family kinases, which are thought to be the enzymes phosphorylating this region *in vivo* (7,8), induced growth arrest and apoptosis in BCR-ABL-transformed cells (11).

In the present study, we performed a database analysis to identify phosphorylated SH3 domains in the human proteome. Four major tyrosine phosphorylation sites were found; all affecting conserved tyrosine residues in positions N, M1, M2, and C of the ligand binding groove (see Fig. 1/A). The SH3 domains of ABL1 and ABL2 kinases were used to investigate the functional and structural effects of tyrosine phosphorylation of the two most prominent sites, N (Tyr89 in ABL1 and Tyr 116 in ABL2) and C (Tyr134 in ABL1 and Tyr 161 in ABL2), using classical biochemical binding assays, ^{1}H-^{15}N NMR spectroscopy, CD spectroscopy, DLS, SAXS and X-ray crystallography. To the best of our knowledge, these are the first phosphorylated SH3 domain structures published so far. Comparison of

phosphorylated, non-phosphorylated and ligand-bound ABL SH3 structures revealed no large-scale structural rearrangements, however, ligand binding was strongly inhibited by either of the introduced phosphate groups. These were sterically blocking the binding groove making it physically inaccessible for the ligands. Phosphorylation of homologous tyrosine residues in other SH3 domains might block ligand binding through a similar molecular level mechanism in general.

Results

Identification of conserved tyrosine phosphorylation sites within human SH3 domains

To assess the importance of tyrosine phosphorylation among SH3 domains and identify novel potential regulatory sites, all human SH3 sequences were aligned (Table S1) and subsequently filtered by the occurrence of tyrosine phosphorylation (using the PhosphoSitePlus database; Table S2). We found 168 individual tyrosine phosphorylation sites in 94 different human SH3 domains. Phosphorylation sites were mapped onto the aligned sequences (Table S2). The four most prominent sites are highlighted on the sequence logo representation of the alignment (Fig. 2). Note that all of these modifications affect positions N (10), M1 (12), M2 (50), and C (55) of the ligand binding groove (see Fig. 1/A). The unfiltered multiple alignment demonstrates that tyrosine residues in these positions are well conserved (Table S1). The specific occurrence of Tyr at positions N, M1, M2, and C among human SH3 domains is 43.2%, 52.0%, 15.0%, and 53.5%, respectively.

The two most common tyrosine phosphorylation sites are positions N and C with 32 and 35 occurrences in the database, respectively. These residues are located in close proximity to each other in the binding grooves of SH3 domains (see Fig. 1/A) and their aromatic rings form the hydrophobic "Pocket I". We found two other major phosphorylation sites at positions M1 and M2 with 13 and 20 occurrences, respectively. These residues are also important in the formation of the ligand binding groove. The overlap of major phosphorylation sites with key structural elements of the binding groove strongly suggests that phosphorylation of either one or more tyrosine(s) at position(s) N, M1, M2, and C, hereinafter referred to as "TyrN", "TyrM1", "TyrM2", and "TyrC", respectively, might inhibit ligand binding.

In vitro phosphorylation of the SH3 domain of ABL1 and ABL2

First, we were screening for tyrosine kinases that can be expressed in an active form in *E. coli* and can be used to catalyze the selective phosphorylation of our SH3 domains. Briefly, kinase domains from distant tyrosine-kinase families (SRC, ABL, Ephrin, Tec) were tested both as His-tagged and GST-tagged proteins. We observed acceptable expression levels of autophosphorylated, active His-EphB1, His-HCK, and GST-ABL1 (data not shown). Both ABL1 SH3 and ABL2 SH3 were selectively and effectively phosphorylated by His-EphB1 at TyrN and TyrC (Fig. 1/B) as it was shown by the combination of anion exchange chromatography and mass spectrometry (Fig. S1). Even after extensive incubation in the presence of excess ATP, tyrosine residues outside of the binding groove (Tyr139 in ABL2 or Tyr112 in ABL1) were not phosphorylated at detectable levels in our experiments. Kinase Reactions were scaled up to obtain doubly-phosphorylated ABL1 SH3 and ABL2 SH3 (referred to as ABL1 $SH3^{pYn/pYc}$ and ABL2 $SH3^{pYn/pYc}$ throughout this work, respectively) on a milligram scale (see Materials and Methods). As we could not achieve acceptable separation of the monophosphorylated SH3 domains (Fig. S1), the following tyrosine-to-phenylalanine mutants were generated: ABL1 $SH3^{Tyr89Phe}$, ABL1 $SH3^{Tyr134Phe}$, ABL2 $SH3^{Tyr116Phe}$, and ABL2 $SH3^{Tyr161Phe}$, referred to as ABL1 $SH3^{YnF}$, ABL1 $SH3^{YcF}$, ABL2 $SH3^{YnF}$, and ABL2 $SH3^{YcF}$, respectively (Fig. 1/C). With this approach, the effects of the two individual phosphorylation events could be investigated separately. Importantly, each phosphorylated Tyr-to-Phe mutant was eluted as a single peak from our anion exchange column (data not shown) corresponding to a singly-phosphorylated protein as shown by mass spectrometry. The lack of chromatographic peaks corresponding to doubly-phosphorylated variants showed that EphB1 is indeed specific for binding groove tyrosines.

Tyrosine-phosphorylation strongly interferes with binding of ABL1 SH3 and ABL2 SH3 to peptide ligands derived from 3BP-2 and ABI2

The intrinsic tryptophan fluorescence intensity signal was used to determine binding affinities of *in vitro* phosphorylated and non-phosphorylated ABL1 and ABL2 SH3 domains for peptide ligands corresponding to proline-rich motifs of 3BP-2 and ABI2 (HPPAYPPPPVPT and TPPTQKPPSPPMS, respectively), known binding partners of ABL1 (12,13). A remarkable blue shift was observed in the spectra of both ABL1 SH3 and ABL2 SH3 upon addition of the ligands (Fig. 3/A). As the highest difference in the fluorescence intensity between the ligand-bound and free SH3 domains was observed at 318 nm, we followed all titrations at this wavelength. Phosphorylation of wild-type ABL1 and ABL2 SH3 domains at both tyrosines resulted in total loss of ligand binding (Fig. 3/B and 3/C). Dissociation constants obtained for Tyr-to-Phe mutants (3BP-2: ~4 to 11 μM, ABI2: ~100 to 200 μM) were generally close to those obtained for wild-type proteins (3BP-2: ~ 2 μM, ABI2: ~100 to 150 μM) showing that the introduced mutations had only minor effects on ligand binding (Table 1). ABL1 $SH3^{YnF/pYc}$ and ABL2 $SH3^{YnF/pYc}$ showed no interaction with either of the ligands. A strong inhibition of ligand binding was also observed in the case of ABL1 $SH3^{pYn/YcF}$ and ABL2 $SH3^{pYn/YcF}$, however, some "residual" binding could be detected (3BP-2: K_d > 100 μM, ABI2: very weak).

Crystal structures of tyrosine-phosphorylated ABL1 and ABL2 SH3 domains reveal atomic level details of the inhibition of ligand binding

To obtain atomic-level insights into the mechanism of inhibition and to understand the somewhat different impact of the two phosphorylation events on ligand binding, we crystallized the doubly-phosphorylated SH3 domains ABL1 $SH3^{pYn/pYc}$ and ABL2 $SH3^{pYn/pYc}$ and the non-phosphorylated ABL2 SH3 as no atomic resolution structure of this domain had been reported previously. Crystal structures were solved at 1.6 Å, 1.4 Å, and 2.0 Å resolutions, respectively (Fig. 4). Crystallographic statistics are reported in Table S3.

The sequences of the SH3 domains of ABL1 and ABL2 are highly similar. There are only four different residues in the βc strand and one in the N-Src loop: Cys119, Ala121, Gln122, Thr123, and His114 in ABL1 correspond to Ser146, Val148, Arg149, Ser150, and Gln141 in ABL2, respectively (see Fig. 1/B). By comparing the ABL1 and ABL2 SH3 domain structures (Fig. S2), it seems unlikely that these differences could significantly influence the structure or function of the ligand binding groove. The most significant differences based on Cα-Cα distances can be found in the RT- ("SGD" region) and distal loops ("TKNG" and "SKNG" regions in ABL1 and ABL2, respectively) (Fig. S2), however, it seems very likely that different crystal contacts are the determining factor here.

With the comparison of the phosphorylated SH3 domains to their non-phosphorylated counterparts, no large-scale structural rearrangements could be observed (Fig. 4). We could only see slight differences in certain regions (e.g. "VASGDN" region in the RT-loop and "KN" region in the distal loop, Fig. S2), however, these again seem to be more related to differences in crystal contacts rather than being the result of tyrosine phosphorylation. Moreover, there are no differences in sidechain conformations that could be obviously interpreted as the result of tyrosine phosphorylation.

To understand the regulatory effect of phosphorylation on ligand binding, we aligned the phosphorylated SH3 structures to a ligand-bound ABL1 SH3 structure (PDB: 1ABO (14), Fig. 5/A). This comparison clearly showed that the phosphate group of pTyrC occupies the center of the binding groove changing the hydrophobic character of two neighboring pockets (Pocket I and II) to hydrophilic, thus making it impossible for the protein to accommodate the ligand in the right position (Fig. 5/B). As ligand binding would result in serious steric clashes between the peptide backbone and the phosphate group, it is not surprising that this modification has a very strong inhibitory effect (see Fig. 3/B and 3/C). The phosphate group of pTyrN is located at the edge of the binding groove (Fig. 5/A). Although it is pointing outwards, it still occupies some space that would be necessary for the peptide backbone to bind (in Pocket I). The somewhat weaker

inhibition in this case (Fig. 3/B and 3/C) might be explained by the higher flexibility of this sidechain (see the different conformations in the two crystallographic monomers) and the greater distance of the phosphate oxygens from the peptide backbone (Fig. 5/C). Moreover, the presence of this phosphate group affects mainly the C-terminal end of the peptide, potentially allowing some "residual" interaction with other parts of the binding groove.

Tyrosine-phosphorylation does not significantly affect the structure of ABL1 SH3 and ABL2 SH3 in solution

To show that the introduced phosphate groups or Tyr-to-Phe mutations did not induce significant structural changes in solution, we acquired far-UV CD spectra of all SH3 derivatives (Fig. S3) and determined the secondary structure contents by BeStSel (http://bestsel.elte.hu/) (Table S4). All studied SH3 variants were nearly exclusively comprised of relaxed and right-twisted antiparallel beta-sheets (~10 and ~18 residues, respectively), turns (~5 residues) and other structures (~27 residues), while no helices, parallel or left-twisted antiparallel beta-sheets were observed. The fact that only slight differences were detected in the secondary structure contents strongly suggests that the three-dimensional structure of ABL1 SH3 and ABL2 SH3 is neither significantly affected by the mutations, nor by phosphorylation.

Similarly, ^{1}H-^{15}N HSQC spectra of non-phosphorylated and phosphorylated ABL1 SH3 derivatives (Fig. S4) indicate only minor structural perturbations upon tyrosine phosphorylation (Fig. S5) showing that the overall structural integrity of the protein was not affected by these molecular level alterations. The behavior of the N- and C-terminal regions (Phe85-Thr102 and Ser132-Val138, respectively) seem to be correlated as phosphorylation of either TyrN or TyrC mutually affects the environment of the other. This is manifested in a similar overall pattern of phosphorylation-induced chemical shift changes over the SH3 sequence for each investigated derivative with most pronounced changes occurring if both residues are phosphorylated. This correlation and synergism most likely arise from the spatial proximity of TyrN and TyrC as they are located close to each other within the ligand binding groove forming the same "functional unit" (Pocket I) of the domain.

SH3 domain tyrosine-phosphorylation does not regulate the dimerization of ABL kinases

ABL1 have been shown to oligomerize at high levels of expression in COS cells (15). Moreover, dimerization of the full length ABL kinases might promote their activation (16-18). As an introduced phosphate group may promote (or interfere with) the formation of dimers/oligomers, and several SH3 domains have already been shown to form homodimers by different mechanisms (19-22), we assessed the effect of phosphorylation on the oligomeric state of ABL1 SH3 and ABL2 SH3. We found that pTyrN was indeed involved in crystal contacts in both the crystal structures of ABL1 SH3$^{pYn/pYc}$ and ABL2 SH3$^{pYn/pYc}$ (Fig. S6). This residue forms a salt bridge with a Lys residue (Lys103 in ABL1, Lys130 in ABL2) of a symmetry-related molecule, indicating a possible monomer-dimer equilibrium that may exist in solution and might be regulated by phosphorylation of TyrN. Moreover, all four crystal structures (ABL1 SH3, ABL2 SH3, ABL1 SH3$^{pYn/pYc}$, ABL2 SH3$^{pYn/pYc}$, PDB: 4jjc, 5np3, 5np2, 5np5, respectively) shared a very similar hydrophobic crystal contact surface built by the same cluster of residues that seemed ideal for forming homodimers (Fig. S6).

However, both small angle X-ray scattering (SAXS) and dynamic light scattering (DLS) analysis showed that the radius of gyration (R_g) of ABL1 SH3 increased by only ~0.1 nm upon phosphorylation. This is consistent with the incorporation of the phosphate groups, but not with dimerization (Fig. S7, Table S5). Direct comparison of our crystal structure with the SAXS profile assuming a monomer-dimer equilibrium model indicated ~10% and ~20% dimeric fraction for ABL1 SH3 and ABL1 SH3$^{pYn/pYc}$, respectively (chi^2~0.8). The fact that neither the protein concentration (data not shown), nor phosphorylation shifted the monomer-to-dimer ratio effectively in these experiments suggests that dimerization of this SH3 domain is not regulated by tyrosine-phosphorylation and the observed dimeric fraction was most likely the result of non-specific protein aggregation.

To complement these studies, oligomerization was further investigated by NMR relaxation experiments (Figure S8, Table S6). Phosphorylation resulted in a slight perturbation of atomic relaxation rates of ABL1 SH3 with no measurable effect on macroscopic dynamic properties. Singly-phosphorylated variants (ABL1 $SH3^{YnF/pYc}$ and ABL1 $SH3^{pYn/YcF}$) showed a similar behavior. The highly similar relaxation properties are manifested in nearly identical values of rotational correlation times (τ_c) for the four ABL1 SH3 variants (Table S6) corresponding to the expected value for a ~7 kDa globular protein in aqueous buffer. Based on τ_c, R_g was calculated for all SH3 variants. A good correlation between the DLS/SAXS- and NMR-derived parameters was found, although, DLS and SAXS slightly overestimated R_g. This is most likely explained by the fact that while the DLS and SAXS derived parameters are affected by the presence of oligomers, the NMR-derived parameters reflect solely the properties of the monomeric fraction. The oligomeric fraction might be heterogenous and thus not be detectable in NMR.

We conclude that neither the phosphorylation of pTyrN nor the phosphorylation of pTyrC changes the monomeric state of ABL1 SH3 (or ABL2 SH3, data not shown) in solution.

Discussion

Identification of major regulatory tyrosine phosphorylation sites in SH3 domains

In this work, we performed a database analysis for tyrosine phosphorylation in SH3 domains. A previous study identified TyrN within the conserved "ALpYDY" motif as the most preferred phosphorylation site (4). Here we found that TyrC within the "YFPSNpYV" motif (Fig. 2) is another prominent site, with even more occurrences in the human phosphoproteome (Table 2 and Table S2). Our experimental strategy allowed us to obtain phosphorylated SH3 domains in large quantities that meet the requirements of *in vitro* biochemical and even structural studies. We observed that phosphorylation of either TyrN or TyrC in the SH3 domain of ABL1 or ABL2 interferes with partner binding. Simultaneous phosphorylation of both residues, which is catalyzed by several Src-family kinases *in vivo*, has a similar effect (8). In other human SH3 domains, phosphorylation not only occurs most frequently on these tyrosine residues, but in many cases, both modifications were observed in the same protein (See Table 2 and Table S2). All these findings strongly suggest that tyrosine kinases may generally accept both TyrN and TyrC as substrates and phosphorylation of one of these residues does not interfere with the phosphorylation of the other.

Effects of TyrC phosphorylation

Phosphorylation of TyrC resulted in total inhibition of ligand binding in our experiments. As TyrC lies between two hydrophobic binding pockets in the middle of the binding groove, the introduced phosphate group fully occupies the space that would be necessary for ligands with polyproline-type II helix conformation. In agreement with this, all TyrC-type phosphorylation events are known to inhibit partner binding in other proteins. For example, the EGF-induced phosphorylation of cortactin SH3 disrupts the interaction with TIP150 (23). Phosphorylation of TyrC in the C-terminal SH3 domain of GRB2 by BCR-ABL or EGFR, results in the inhibition of Sos binding (24). This mechanism represents a negative regulatory loop limiting EGF-mediated signaling in time (24) and also allows other signaling pathways to antagonize EGF-induced MAP kinase activation and cell proliferation (25,26). Phosphorylation of TyrC in VAV1 SH3 interferes with autoinhibitory intramolecular interactions leading to the activation of the protein (27).

Effects of TyrN phosphorylation

Phosphorylation of TyrN was found to inhibit ligand binding significantly in this work (see Fig. 3/B and 3/C). Interestingly, while this modification in Endophilin A2 is known to disrupt the interaction with dynamin (28,29), it does not inhibit the interaction with FAK (28). Moreover, TyrN-type phosphorylation of the adaptor protein ABI1 seems to enhance the interaction with ABL1 (30). Phosphorylation of TyrN in the Tec family tyrosine-kinase BTK was found to inhibit binding to WASP while not influencing the interaction with c-Cbl and was even required for the interaction with kinase-active SYK (31). These observations indicate that TyrN (and maybe TyrC) phosphorylation can be part of more complex

molecular level mechanisms *in vivo*. For example, other regulated domain-level interactions may exist in parallel in multidomain proteins and their complexes that depend on the inhibition of SH3 domain function. TyrN phosphorylation might also be involved in the activation of autoregulated multidomain-proteins by disrupting autoinhibitory intramolecular interactions. One example is the Tec-family tyrosine-kinase ITK, where TyrN phosphorylation extends the duration of kinase activation (32,33). This modification and also the phosphorylation of the homologous site in BTK may serve as "checkpoints" altering the interaction profile of these kinases with other proteins, thereby controlling the transition between early and late activation events (32,34,35).

Regulation of ABL kinases by SH3 domain tyrosine phosphorylation

Here, we presented the crystal structures of two closely related tyrosine-phosphorylated SH3 domains: ABL1 $SH3^{pYn/pYc}$ and ABL2 $SH3^{pYn/pYc}$. Only minor changes were observed in the structures upon phosphorylation; however, the ability of the SH3 domains to bind peptide ligands was compromised by the phosphate groups, mainly by steric blocking of the binding groove. Activity of the kinase domain in ABL1 and ABL2 are regulated by autoinhibition (36,37). In the "closed", inactive conformation, the SH3 domain binds to the proline-rich linker between the SH2 and kinase domains (36,37). Tyrosine phosphorylation within the ligand binding groove of the SH3 domain disrupts this interaction *in vivo* (7,8). Although we could not observe any interaction between the recombinant ABL1 and ABL2 SH3 domains and a synthetic peptide corresponding to this linker in our experiments (data not shown), our results demonstrate that either the phosphorylation of TyrN or TyrC strongly interferes with ligand binding. Phosphorylation of any of these residues or both may likely lead to the activation of ABL kinases and inhibit their SH3-mediated interactions with external ligands. Interestingly, while the non-receptor tyrosine kinase SRC is regulated by a similar autoinhibitory mechanism, phosphorylation of TyrC only inhibits partner binding but not required for the activation of the kinase (38).

Although our crystal structures raised the possibility of a monomer–dimer equilibrium regulated by the phosphorylation of TyrN, we demonstrated by DLS, SAXS, and NMR that neither the phosphorylation of TyrN nor the phosphorylation of TyrC affects the monomeric state of these domains in solution.

No phosphorylation of Tyr112 in ABL1 or Tyr139 in ABL2 was observed in this study. These residues are not part of the ligand binding groove and they do not contribute to any intramolecular interaction necessary for the formation of the autoinhibited conformation of ABL kinases (37). Therefore, it seems to be unlikely that there is any effect associated with their phosphorylation on the known functions of ABL1 SH3 or ABL2 SH3, including the binding of external ligands. To the best of our knowledge, there has been no information reported on the regulatory functions of these phosphorylation events so far.

Summary

In this work, we recognized novel major tyrosine phosphorylation sites in the binding groove of SH3 domains and demonstrated that SH3 domain tyrosine phosphorylation strongly inhibits the interaction with proline-rich ligands due to the steric blocking of the ligand binding groove by the phosphate groups. Phosphorylation is not followed by significant structural rearrangements or oligomerization of the domains. Based on the occurrence of phosphotyrosine residues in homologous positions of many human SH3 domains, this seems to be a widespread mechanism regulating a significant part of the SH3-interactome in cells.

Note. While this manuscript was being prepared for publication, an article by Dionne et al. (39) appeared reporting the phosphorylation of TyrC residues in the SH3 domains of NCK by the receptor tyrosine kinase Eph4a. Their findings confirm our conclusions showing that phosphorylation of TyrC inhibits ligand binding and functions as a negative regulatory loop through which receptor tyrosine kinases terminate signaling.

Experimental procedures

Sequence analysis of SH3 domains and identification of phosphorylation sites

Sequences of human SH3 domains were obtained from UniProt (40) and subsequently aligned by Clustal Omega (41). The alignment was reviewed and the boundaries of SH3 domains were corrected manually. Tyrosine phosphorylation sites were mapped based on both high- and low-throughput data from PhosphoSitePlus (42). All non-phosphorylated SH3 domain sequences were removed and the resulting multiple alignment was used as a template to generate a sequence logo by using WebLogo (43).

DNA constructs

The TEV protease gene cloned into a bacterial expression vector was a kind gift of Dr. László Nyitray. DNA constructs harboring the coding region of human ABL1, ABL2 and EphB1 kinases were obtained from Addgene. Sequences corresponding to the SH3 domain of ABL1 (Uniprot accession number: P00519, residues: 64-120) and ABL2 (Uniprot accession number: P42684, residues: 110-166) and the kinase domain of EphB1 receptor (Uniprot accession number: P54762, residues: 612-892) were amplified by PCR and subcloned into a modified pET vector encoding a His-tag followed by TEV protease recognition site by using NdeI and BamHI restriction enzymes. Mutants of the ABL1 and ABL2 SH3 domains were generated by PCR by using a third oligonucleotide carrying the base changes necessary for the mutations. All constructs were verified by DNA sequencing (Eurofins Genomics).

Protein expression and purification

Wild-type and mutant SH3 domains of ABL kinases and the kinase domain of EphB1 receptor were expressed in *E. coli* Rosetta pLysS (Novagen) and Arctic Express (Agilent Technologies) cells, respectively. Cells were grown in 2YT medium up to OD_{600} = 0.7 at 37 °C and induced overnight with 0.5 mM IPTG at 16 °C. The ^{15}N–enriched SH3 domains were expressed in *E. coli* Rosetta pLysS cells. Cultures were grown in 4 × 1000 ml 2YT medium up to OD_{600} = 0.7 at 37 °C. Cells were harvested by centrifugation and resuspended in 1 l Minimal Medium containing 1 g/l ^{15}N–NH_4Cl and induced by 0.5 mM IPTG at 37 °C for 4 h. Purification of all proteins followed the same protocol. After centrifugation, cells were resuspended in lysis buffer (50 mM Na_2HPO_4, 500 mM NaCl, 0.25 mM TCEP, pH = 8.0) and subsequently lysed by lysozyme treatment, one freeze-thaw cycle, and sonication. Proteins were purified by immobilized metal affinity chromatography by using Profinity™ IMAC Ni-charged Resin (BioRad). Fractions containing the protein of interest were pooled and subsequently dialyzed against lysis buffer. His-tags were cleaved by TEV protease digestion. To remove the protease, residual undigested protein molecules and digested His-tags, samples were loaded again onto a Ni-charged IMAC column. The flow-through was collected, dialyzed against buffer "A" (20 mM TRIS, pH = 8.0) and further purified by anion exchange chromatography (HiTrapQ column) applying a linear gradient of buffer "B" (20 mM TRIS, 1M NaCl, pH = 8.0). Finally, protein samples were dialyzed against TRIS Buffered Saline (TBS) supplemented with TCEP (20 mM TRIS, 150 mM NaCl, 0.5 mM TCEP, pH = 7.6), concentrated by ultrafiltration, aliquoted and stored at -80 °C.

SH3 domain phosphorylation

In vitro kinase reactions were performed by the recombinant kinase domain of EphB1 receptor in a buffer containing (20 mM TRIS, 150 mM NaCl, 2 mM ATP, 10 mM $MgCl_2$, 0.5 mM TCEP, 0.01% Triton-X 100, pH = 7.6) at 30 °C overnight. Typical concentrations of substrates and the kinase was 500 µM and 10 µM in reaction mixtures, respectively. Reactions were stopped by the addition of 0.5 M EDTA pH = 7.6 (20 µM final concentration). Samples were diluted with Buffer "A" to reach a final NaCl concentration of 15 mM. Phosphorylated SH3 domains were separated by High Performance Liquid Chromatography (HPLC) by using a Sepax Proteomix SAX-NP3 (strong anion exchanger) column and a linear gradient of Buffer "A" and Buffer "B". Fractions were analyzed by mass spectrometry to identify the number of modified tyrosines and their positions within the sequence. (See details in Supporting Information.)

Peptide synthesis

The synthetic peptides corresponding to the SH3 binding motif of 3BP-2 (HPPAYPPPPVPT, Uniprot accession number:

P78314, residues: 200-211) and ABI2 (TPPTQKPPSPPMS, Uniprot accession number: Q9NYB9, residues: 175-187) were obtained from GeneScript. The N- and C-termini of the peptides were acetylated and amidated, respectively.

Ligand binding assays (fluorescence spectroscopy)

Titrations of the ABL1 and ABL2 SH3 domains by peptide ligands corresponding to the ABL1 SH3-binding linear motif of 3BP-2 and ABI2 (HPPAYPPPPVPT and TPPTQKPPSPPMS, respectively) were followed by the intrinsic tryptophan fluorescence signal. Prior to titrations, SH3 samples were dialyzed against Phosphate Buffered Saline (PBS) supplemented with 0.5 mM TCEP and the peptide ligands were also dissolved in the same buffer. Titrations were performed by pipetting the titrant solution (3BP-2 or ABI2 peptide, 500 µM and 1.7 mM, respectively) in 2 µl steps into the cuvette. The starting volume and concentration of the SH3 solutions in the cuvette was 800 µl and 5 µM, respectively. Experiments were carried out at 25 °C by using a FluoroMax-3 spectrofluorometer (HORIBA Scientific). Excitation of the fluorophores was performed at 295 nm with a spectral bandwidth of 2 nm. Emission scans were acquired in the wavelength range from 310 nm to 400 nm with an emission bandwidth of 2 nm. Titrations were followed at 318 nm (the difference between the fluorescence intensities of the apo- and ligand-bound states was the highest at this wavelength). The average signal intensity and standard deviation of three independent titrations was plotted against the volume of the titrant. Data were fitted by the following equation to determine the dissociation constants:

$$I = a[A]'_t + (b - a)\frac{K_d + [A]'_t + [B]'_t - \sqrt{(K_d + [A]'_t + [B]'_t)^2 - 4[A]'_t[B]'_t}}{2}$$

Where:

$$[A]'_t = \frac{C_A V_A}{V_A + V_B}$$

is the total concentration of the SH3 domain in the cuvette at each point of titration,

$$[B]'_t = \frac{C_B V_B}{V_A + V_B}$$

is the total concentration of the ligand peptide in the cuvette at each point of titration, K_d is the dissociation constant, C_A and C_B are the concentrations of the stock solutions, V_A and V_B are the total volumes of the stock solutions mixed at the given point of titration, *a* and *b* are the theoretical fluorescence intensities of the ABL1 SH3 solution and the ABL1 SH3 - ligand peptide complex solution at one molar concentration, respectively.

CD spectroscopy

Circular Dichroism (CD) spectra were recorded at 25 °C in the wavelength range from 190 nm to 250 nm (1 nm increments) on a JASCO J-715 Circular Dichroism Spectropolarimeter (JASCO Inc.). The scanning speed was set to 20 nm/min and the spectral bandwidth was 2 nm. Protein samples were dialyzed against CD buffer (50 mM phosphate, pH = 7.4) overnight and diluted to a concentration of 20 µM prior to the experiments. The spectrum of the buffer was subtracted from each protein spectrum. Corrected far-UV CD spectra were analyzed by the BeStSel (http://bestsel.elte.hu/) secondary structure prediction server (44).

Protein crystallization

All proteins (ABL2 SH3, ABL2 SH3$^{pY116/pY161}$, ABL1 SH3$^{pY89/pY134}$) were dialyzed twice against TBS supplemented with TCEP and sodium-azide (20 mM TRIS-HCl, 150 mM NaCl, 3 mM NaN_3, 0.5 mM TCEP, pH = 7.6) and concentrated to ~750 µM using Amicon Ultra-15 3K Centrifugal Filter Devices (Millipore). Crystals were grown using the hanging drop vapor diffusion method at 293 K with a reservoir solution of 0.8 M sodium citrate, 0.1 M sodium cacodylate, pH = 6.5 in the case of ABL1 SH3$^{pY89/pY134}$, 1.8 M di-sodium DL-malate, pH = 7.0 in the case of ABL2 SH3 and 1.8 M $(NH_4)_2SO_4$, 0.1 M sodium acetate, pH = 4.6 in the case of ABL2 SH3$^{pY116/pY161}$. Drops were composed of 1 µl reservoir solution and 1 µl protein solution. Crystals were soaked in reservoir solution supplemented with 15% glycerol for ~30 seconds and subsequently cooled in liquid nitrogen.

X-ray diffraction experiments were performed at beamline P13 of the PETRA III synchrotron source (EMBL Hamburg). Data were integrated with XDS (45) and the phase problem was solved by PHASER (46). A high-resolution X-ray structure of ABL1 SH3 was used as

searching model (PDB: 4JJC). The MR search identified 4, 2 and 2 molecules in the asymmetric unit of structure ABL2 SH3, ABL2 SH3$^{pY116/pY161}$ and ABL1 SH3$^{pY89/pY134}$, respectively. Structure refinement was carried out in Phenix (47) and modeling was done in Coot (48). The structures were deposited in PDB under reference codes 5np3, 5np5 and 5np2. Crystallographic data and refinement statistics are shown in Table S3.

Small Angle X-ray Scattering (SAXS) experiments

SAXS experiments were carried out at the BM29 beamline at ESRF, Grenoble. Prior to the measurements, samples were dialyzed against TBS supplemented with 0.5 mM TCEP. A dilution series was measured from 2.8 mg/ml to 0.4 mg/ml to reduce the inter-particle effect from the scattering profile but no concentration dependent changes were observed during data collection. Data were analyzed using the ATSAS program package (49). Primary data was analyzed with PRIMUS (50). Fitting to the monomeric crystal structure was performed with CRYSOL (51) and to fit with the monomer-dimer ensemble we used OLIGOMER (50). The structure of the dimer was assumed to be identical to the crystallographic dimer stabilized by the interactions of pTyr89 in ABL1 SH3 (Fig. S6).

Dynamic Light Scattering

The hydrodynamic size distribution profile was determined by an Avid Nano W130i instrument at 25 °C. Prior to the measurements, samples were dialyzed against TBS supplemented with 0.5 mM TCEP. Protein concentration of ABL1 SH3 and ABL1 SH3$^{pTyr89/134}$ was 5.05 mg/ml and 3.82 mg/ml, respectively. R_g values were calculated from the experimental R_h using the scaling factor 0.775.

NMR spectroscopy

Phosphorylation induced structural changes were monitored by two-dimensional ^{1}H-^{15}N HSQC NMR measurements (52) performed on uniformly [U-^{15}N]-enriched wild type and mutated (Tyr89Phe and Tyr134Phe) ABL1 SH3. Experiments were carried out on a 600 MHz Varian NMR System spectrometer equipped with a 5 mm indirect detection triple resonance (^{1}H^{13}C^{15}N) z-axis gradient probe in PBS buffer pH 7.2 containing 3mM NaN_3 and 0.5 mM TCEP at 25 °C.

Resonance assignment was obtained on uniformly [U-^{15}N]-enriched ABL1 SH3 at 25 °C using a combination of two-dimensional (2D) ^{1}H-^{15}N HSQC (52), three-dimensional (3D) ^{1}H-^{15}N TOCSY-HSQC (τ_m = 120 ms) and ^{1}H-^{15}N NOESY-HSQC (τ_m = 250 ms) (53), 2D ^{1}H-^{1}H TOCSY (τ_m = 120 ms) (54), ^{1}H-^{1}H NOESY (τ_m = 50, 100, 250 ms) (55), and natural abundance ^{1}H-^{13}C HSQC (56) experiments. Spectral processing, computer-assisted spin-system analysis, and resonance assignment were carried out using Felix 2004 (Accelrys, Inc.), To obtain the ^{1}H, ^{15}N assignment of phosphorylated derivatives, the assignment of non-phosphorylated ABL1 SH3 was transferred. Combined (^{1}HN, ^{15}N) chemical shift perturbations were calculated using the equation of $\Delta\delta_{1HN,15N} = \sqrt{[(\Delta\delta^2_{HN}+\Delta\delta^2_{N}/25)/2]}$ (57).

The ^{15}N relaxation measurements (52,58,59) were collected on non-phosphorylated and phosphorylated derivatives (pY89, pY134, pY89pY134) of [U-^{15}N]-enriched ABL1 SH3 at 25 °C at a magnetic field strength of 14.1 T (corresponding to ^{15}N Larmor frequency of 60 MHz). Backbone amide ^{15}N R_1 values were measured from a series of eight spectra with the following relaxation delay times: 50, 100, 170, 240, 340, 480, 630, 800 ms and 50, 100, 170, 240, 420, 610, 720, 800 ms. Amide ^{15}N R_2 values were obtained similarly: 10, 30, 50, 70, 110, 170, 210, 250 ms and 10, 30, 50, 90, 130, 150, 170, 230 ms. Fourier-transformation of free induction decays was performed using Felix 2004 (Accelrys, Inc.). For relaxation analysis, the transformed and phased spectra were imported into CCPNMR. Rotational correlation times (τ_c) were calculated from ^{15}N R_1, R_2 relaxation rates using the corresponding equation in Kay et al. (60) considering the J(0) and J(ωN) spectral density terms. Hydrodynamic radii (R_h) were derived based on the equation of $\tau_c = 4\pi\eta_{H2O}R_h^3/3k_BT$, where η_{H2O} is the viscosity of water, T is the temperature and k_B is the Boltzmann constant.

Acknowledgement: The authors wish to thank László Drahos and Olivér Ozohanics (Instrumentation Center, MTA TTK) for their help in mass spectrometry measurements. Special thanks are due to Mrs. Zita Solti for her assistance in the expression and purification of recombinant proteins. Protein crystallization and in-house X-ray scattering experiments were performed at the Biostruct Laboratory (www.biostruct.org). The authors thank to BioStruct-X for funding the X-ray crystallography and Small angle X-ray scattering measurements in EMBL Hamburg and ESRF Grenoble.

Data availability: The atomic coordinates and structure factors for the ABL2 SH3, ABL2 SH3$^{pY116/pY161}$, and ABL1 SH3$^{pY89/pY134}$ have been deposited to the Protein Data Bank (PDB) under the accession codes 5np3, 5np5 and 5np2. NMR data have been deposited to the BMRB (Biological Magnetic Resonance Data Bank) under the accession codes 27359 and 27362. Source data for biochemical experiments that support the findings of this study are available from the corresponding authors upon reasonable request.

Conflict of interest: The authors declare that they have no conflicts of interest with the contents of this article.

Author contributions: BM carried out the experiments, analyzed data and wrote the paper. LR, VV and LB conceived the project, supervised the research and prepared the manuscript. GG participated in the X-ray and SAXS measurements. OT performed the NMR measurements. KK and BS helped in data analysis and drawing figures. AC and GK assisted in the tryptophan fluorescence-based titrations. MD helped in the generation of recombinant proteins. SS contributed to the *in vitro* phosphorylation experiments. LN helped in writing the manuscript. IL and BV run the Biostruct Laboratory and assisted in the in-house X-ray scattering experiments. All authors analyzed the results and approved the final version of the manuscript.

References

1. Kurochkina, N., and Guha, U. (2013) SH3 domains: modules of protein-protein interactions. *Biophysical reviews* **5**, 29-39
2. Gmeiner, W. H., and Horita, D. A. (2001) Implications of SH3 domain structure and dynamics for protein regulation and drug design. *Cell biochemistry and biophysics* **35**, 127-140
3. Saksela, K., and Permi, P. (2012) SH3 domain ligand binding: What's the consensus and where's the specificity? *FEBS letters* **586**, 2609-2614
4. Tatarova, Z., Brabek, J., Rosel, D., and Novotny, M. (2012) SH3 domain tyrosine phosphorylation--sites, role and evolution. *PloS one* **7**, e36310
5. Bradley, W. D., and Koleske, A. J. (2009) Regulation of cell migration and morphogenesis by Abl-family kinases: emerging mechanisms and physiological contexts. *Journal of cell science* **122**, 3441-3454
6. Greuber, E. K., Smith-Pearson, P., Wang, J., and Pendergast, A. M. (2013) Role of ABL family kinases in cancer: from leukaemia to solid tumours. *Nature reviews. Cancer* **13**, 559-571
7. Chen, S., O'Reilly, L. P., Smithgall, T. E., and Engen, J. R. (2008) Tyrosine phosphorylation in the SH3 domain disrupts negative regulatory interactions within the c-Abl kinase core. *Journal of molecular biology* **383**, 414-423
8. Meyn, M. A., 3rd, Wilson, M. B., Abdi, F. A., Fahey, N., Schiavone, A. P., Wu, J., Hochrein, J. M., Engen, J. R., and Smithgall, T. E. (2006) Src family kinases phosphorylate the Bcr-Abl SH3-SH2 region and modulate Bcr-Abl transforming activity. *The Journal of biological chemistry* **281**, 30907-30916
9. Steen, H., Fernandez, M., Ghaffari, S., Pandey, A., and Mann, M. (2003) Phosphotyrosine mapping in Bcr/Abl oncoprotein using phosphotyrosine-specific immonium ion scanning. *Molecular & cellular proteomics : MCP* **2**, 138-145
10. Srinivasan, D., Kaetzel, D. M., and Plattner, R. (2009) Reciprocal regulation of Abl and receptor tyrosine kinases. *Cellular signalling* **21**, 1143-1150
11. Wilson, M. B., Schreiner, S. J., Choi, H. J., Kamens, J., and Smithgall, T. E. (2002) Selective pyrrolo-pyrimidine inhibitors reveal a necessary role for Src family kinases in Bcr-Abl signal transduction and oncogenesis. *Oncogene* **21**, 8075-8088
12. Ren, R., Mayer, B. J., Cicchetti, P., and Baltimore, D. (1993) Identification of a ten-amino acid proline-rich SH3 binding site. *Science* **259**, 1157-1161
13. Dai, Z., and Pendergast, A. M. (1995) Abi-2, a novel SH3-containing protein interacts with the c-Abl tyrosine kinase and modulates c-Abl transforming activity. *Genes & development* **9**, 2569-2582
14. Musacchio, A., Saraste, M., and Wilmanns, M. (1994) High-resolution crystal structures of tyrosine kinase SH3 domains complexed with proline-rich peptides. *Nature structural biology* **1**, 546-551
15. Fan, P. D., Cong, F., and Goff, S. P. (2003) Homo- and hetero-oligomerization of the c-Abl kinase and Abelson-interactor-1. *Cancer research* **63**, 873-877
16. Woessner, D. W., Eiring, A. M., Bruno, B. J., Zabriskie, M. S., Reynolds, K. R., Miller, G. D., O'Hare, T., Deininger, M. W., and Lim, C. S. (2015) A coiled-coil mimetic intercepts BCR-ABL1 dimerization in native and kinase-mutant chronic myeloid leukemia. *Leukemia* **29**, 1668-1675

17. Maru, Y., Afar, D. E., Witte, O. N., and Shibuya, M. (1996) The dimerization property of glutathione S-transferase partially reactivates Bcr-Abl lacking the oligomerization domain. *The Journal of biological chemistry* **271**, 15353-15357
18. Smith, K. M., and Van Etten, R. A. (2001) Activation of c-Abl kinase activity and transformation by a chemical inducer of dimerization. *The Journal of biological chemistry* **276**, 24372-24379
19. Kristensen, O., Guenat, S., Dar, I., Allaman-Pillet, N., Abderrahmani, A., Ferdaoussi, M., Roduit, R., Maurer, F., Beckmann, J. S., Kastrup, J. S., Gajhede, M., and Bonny, C. (2006) A unique set of SH3-SH3 interactions controls IB1 homodimerization. *The EMBO journal* **25**, 785-797
20. Levinson, N. M., Visperas, P. R., and Kuriyan, J. (2009) The tyrosine kinase Csk dimerizes through Its SH3 domain. *PloS one* **4**, e7683
21. Ross, B., Kristensen, O., Favre, D., Walicki, J., Kastrup, J. S., Widmann, C., and Gajhede, M. (2007) High resolution crystal structures of the p120 RasGAP SH3 domain. *Biochem Biophys Res Commun* **353**, 463-468
22. Matsumura, Y., Shinjo, M., Matsui, T., Ichimura, K., Song, J., and Kihara, H. (2013) Structural study of hNck2 SH3 domain protein in solution by circular dichroism and X-ray solution scattering. *Biophysical chemistry* **175-176**, 39-46
23. Adams, G., Jr., Zhou, J., Wang, W., Wu, H., Quan, J., Liu, Y., Xia, P., Wang, Z., Zhou, S., Jiang, J., Mo, F., Zhuang, X., Thomas, K., Hill, D. L., Aikhionbare, F. O., He, P., Liu, X., Ding, X., and Yao, X. (2016) The Microtubule Plus End Tracking Protein TIP150 Interacts with Cortactin to Steer Directional Cell Migration. *The Journal of biological chemistry* **291**, 20692-20706
24. Li, S., Couvillon, A. D., Brasher, B. B., and Van Etten, R. A. (2001) Tyrosine phosphorylation of Grb2 by Bcr/Abl and epidermal growth factor receptor: a novel regulatory mechanism for tyrosine kinase signaling. *The EMBO journal* **20**, 6793-6804
25. Haines, E., Minoo, P., Feng, Z., Resalatpanah, N., Nie, X. M., Campiglio, M., Alvarez, L., Cocolakis, E., Ridha, M., Di Fulvio, M., Gomez-Cambronero, J., Lebrun, J. J., and Ali, S. (2009) Tyrosine phosphorylation of Grb2: role in prolactin/epidermal growth factor cross talk in mammary epithelial cell growth and differentiation. *Molecular and cellular biology* **29**, 2505-2520
26. Anselmi, F., Orlandini, M., Rocchigiani, M., De Clemente, C., Salameh, A., Lentucci, C., Oliviero, S., and Galvagni, F. (2012) c-ABL modulates MAP kinases activation downstream of VEGFR-2 signaling by direct phosphorylation of the adaptor proteins GRB2 and NCK1. *Angiogenesis* **15**, 187-197
27. Barreira, M., Fabbiano, S., Couceiro, J. R., Torreira, E., Martinez-Torrecuadrada, J. L., Montoya, G., Llorca, O., and Bustelo, X. R. (2014) The C-terminal SH3 domain contributes to the intramolecular inhibition of Vav family proteins. *Science signaling* **7**, ra35
28. Wu, X., Gan, B., Yoo, Y., and Guan, J. L. (2005) FAK-mediated src phosphorylation of endophilin A2 inhibits endocytosis of MT1-MMP and promotes ECM degradation. *Developmental cell* **9**, 185-196
29. Fan, H., Zhao, X., Sun, S., Luo, M., and Guan, J. L. (2013) Function of focal adhesion kinase scaffolding to mediate endophilin A2 phosphorylation promotes epithelial-mesenchymal transition and mammary cancer stem cell activities in vivo. *The Journal of biological chemistry* **288**, 3322-3333

30. Sato, M., Maruoka, M., Yokota, N., Kuwano, M., Matsui, A., Inada, M., Ogawa, T., Ishida-Kitagawa, N., and Takeya, T. (2011) Identification and functional analysis of a new phosphorylation site (Y398) in the SH3 domain of Abi-1. *FEBS letters* **585**, 834-840
31. Morrogh, L. M., Hinshelwood, S., Costello, P., Cory, G. O., and Kinnon, C. (1999) The SH3 domain of Bruton's tyrosine kinase displays altered ligand binding properties when auto-phosphorylated in vitro. *European journal of immunology* **29**, 2269-2279
32. Wilcox, H. M., and Berg, L. J. (2003) Itk phosphorylation sites are required for functional activity in primary T cells. *The Journal of biological chemistry* **278**, 37112-37121
33. Andreotti, A. H., Bunnell, S. C., Feng, S., Berg, L. J., and Schreiber, S. L. (1997) Regulatory intramolecular association in a tyrosine kinase of the Tec family. *Nature* **385**, 93-97
34. Wahl, M. I., Fluckiger, A. C., Kato, R. M., Park, H., Witte, O. N., and Rawlings, D. J. (1997) Phosphorylation of two regulatory tyrosine residues in the activation of Bruton's tyrosine kinase via alternative receptors. *Proceedings of the National Academy of Sciences of the United States of America* **94**, 11526-11533
35. Nisitani, S., Kato, R. M., Rawlings, D. J., Witte, O. N., and Wahl, M. I. (1999) In situ detection of activated Bruton's tyrosine kinase in the Ig signaling complex by phosphopeptide-specific monoclonal antibodies. *Proceedings of the National Academy of Sciences of the United States of America* **96**, 2221-2226
36. Barila, D., and Superti-Furga, G. (1998) An intramolecular SH3-domain interaction regulates c-Abl activity. *Nature genetics* **18**, 280-282
37. Nagar, B., Hantschel, O., Young, M. A., Scheffzek, K., Veach, D., Bornmann, W., Clarkson, B., Superti-Furga, G., and Kuriyan, J. (2003) Structural basis for the autoinhibition of c-Abl tyrosine kinase. *Cell* **112**, 859-871
38. Broome, M. A., and Hunter, T. (1997) The PDGF receptor phosphorylates Tyr 138 in the c-Src SH3 domain in vivo reducing peptide ligand binding. *Oncogene* **14**, 17-34
39. Dionne, U., Chartier, F. J. M., Lopez de Los Santos, Y., Lavoie, N., Bernard, D. N., Banerjee, S. L., Otis, F., Jacquet, K., Tremblay, M. G., Jain, M., Bourassa, S., Gish, G. D., Gagne, J. P., Poirier, G. G., Laprise, P., Voyer, N., Landry, C. R., Doucet, N., and Bisson, N. (2018) Direct Phosphorylation of SRC Homology 3 Domains by Tyrosine Kinase Receptors Disassembles Ligand-Induced Signaling Networks. *Molecular cell* **70**, 995-1007 e1011
40. (2017) UniProt: the universal protein knowledgebase. *Nucleic acids research* **45**, D158-D169
41. Sievers, F., Wilm, A., Dineen, D., Gibson, T. J., Karplus, K., Li, W., Lopez, R., McWilliam, H., Remmert, M., Soding, J., Thompson, J. D., and Higgins, D. G. (2011) Fast, scalable generation of high-quality protein multiple sequence alignments using Clustal Omega. *Molecular systems biology* **7**, 539
42. Hornbeck, P. V., Kornhauser, J. M., Tkachev, S., Zhang, B., Skrzypek, E., Murray, B., Latham, V., and Sullivan, M. (2012) PhosphoSitePlus: a comprehensive resource for investigating the structure and function of experimentally determined post-translational modifications in man and mouse. *Nucleic acids research* **40**, D261-270
43. Crooks, G. E., Hon, G., Chandonia, J. M., and Brenner, S. E. (2004) WebLogo: a sequence logo generator. *Genome research* **14**, 1188-1190

44. Micsonai, A., Wien, F., Kernya, L., Lee, Y. H., Goto, Y., Refregiers, M., and Kardos, J. (2015) Accurate secondary structure prediction and fold recognition for circular dichroism spectroscopy. *Proceedings of the National Academy of Sciences of the United States of America* **112**, E3095-3103
45. Kabsch, W. (2010) Xds. *Acta crystallographica. Section D, Biological crystallography* **66**, 125-132
46. McCoy, A. J., Grosse-Kunstleve, R. W., Adams, P. D., Winn, M. D., Storoni, L. C., and Read, R. J. (2007) Phaser crystallographic software. *Journal of applied crystallography* **40**, 658-674
47. Adams, P. D., Afonine, P. V., Bunkoczi, G., Chen, V. B., Davis, I. W., Echols, N., Headd, J. J., Hung, L. W., Kapral, G. J., Grosse-Kunstleve, R. W., McCoy, A. J., Moriarty, N. W., Oeffner, R., Read, R. J., Richardson, D. C., Richardson, J. S., Terwilliger, T. C., and Zwart, P. H. (2010) PHENIX: a comprehensive Python-based system for macromolecular structure solution. *Acta crystallographica. Section D, Biological crystallography* **66**, 213-221
48. Emsley, P., Lohkamp, B., Scott, W. G., and Cowtan, K. (2010) Features and development of Coot. *Acta crystallographica. Section D, Biological crystallography* **66**, 486-501
49. Petoukhov, M. V., Franke, D., Shkumatov, A. V., Tria, G., Kikhney, A. G., Gajda, M., Gorba, C., Mertens, H. D., Konarev, P. V., and Svergun, D. I. (2012) New developments in the ATSAS program package for small-angle scattering data analysis. *Journal of applied crystallography* **45**, 342-350
50. Konarev, P. V., Volkov, V. V., Sokolova, A. V., Koch, M. H. J., and Svergun, D. I. (2003) PRIMUS: a Windows PC-based system for small-angle scattering data analysis. *Journal of applied crystallography* **36**, 1277-1282
51. Svergun, D., Barberato, C., and Koch, M. H. J. (1995) CRYSOL - a Program to Evaluate X-ray Solution Scattering of Biological Macromolecules from Atomic Coordinates. *Journal of applied crystallography* **28**, 768-773
52. Kay, L., Keifer, P., and Saarinen, T. (1992) Pure absorption gradient enhanced heteronuclear single quantum correlation spectroscopy with improved sensitivity. *Journal of the American Chemical Society* **114**, 10663-10665
53. Marion, D., Kay, L. E., Sparks, S. W., Torchia, D. A., and Bax, A. (1989) Three-dimensional heteronuclear NMR of nitrogen-15 labeled proteins. *Journal of the American Chemical Society* **111**, 1515-1517
54. Bax, A., and Davis, D. G. (1985) MLEV-17-based two-dimensional homonuclear magnetization transfer spectroscopy. *Journal of Magnetic Resonance* **65**, 355-360
55. Kumar, A., Ernst, R. R., and Wüthrich, K. (1980) A two-dimensional nuclear Overhauser enhancement (2D NOE) experiment for the elucidation of complete proton-proton cross-relaxation networks in biological macromolecules. *Biochemical and Biophysical Research Communications* **95**, 1-6
56. John, B. K., Plant, D., Webb, P., and Hurd, R. E. (1992) Effective combination of gradients and crafted RF pulses for water suppression in biological samples. *Journal of Magnetic Resonance* **98**, 200-206
57. Grzesiek, S., Bax, A., Clore, G. M., Gronenborn, A. M., Hu, J. S., Kaufman, J., Palmer, I., Stahl, S. J., and Wingfield, P. T. (1996) The solution structure of HIV-1 Nef reveals an unexpected fold and permits delineation of the binding surface for the SH3 domain of Hck tyrosine protein kinase. *Nature structural biology* **3**, 340-345

58. Kay, L. E., Nicholson, L. K., Delaglio, F., Bax, A., and Torchia, D. A. (1992) Pulse sequences for removal of the effects of cross correlation between dipolar and chemical-shift anisotropy relaxation mechanisms on the measurement of heteronuclear T1 and T2 values in proteins. *Journal of Magnetic Resonance* **97**, 359-375
59. Farrow, N. A., Muhandiram, R., Singer, A. U., Pascal, S. M., Kay, C. M., Gish, G., Shoelson, S. E., Pawson, T., Forman-Kay, J. D., and Kay, L. E. (1994) Backbone dynamics of a free and phosphopeptide-complexed Src homology 2 domain studied by 15N NMR relaxation. *Biochemistry* **33**, 5984-6003
60. Kay, L. E., Torchia, D. A., and Bax, A. (1989) Backbone dynamics of proteins as studied by 15N inverse detected heteronuclear NMR spectroscopy: application to staphylococcal nuclease. *Biochemistry* **28**, 8972-8979

FOOTNOTES

This work was supported by a grant from the National Research, Development and Innovation Fund of Hungary (K 124045 and FIEK_16-1-2016-0005) and the MedinProt Program of the Hungarian Academy of Sciences (to LB), the National Research, Development and Innovation Office grant K-109035 and the 'János Bolyai Research Scholarship' Program of the Hungarian Academy of Sciences (to OT and VV) and the 'MTA Postdoctoral Fellowship Programme' of the Hungarian Academy of Sciences (to LR and VV).

Table 1. Dissociation constants determined by intrinsic tryptophan fluorescence-based titrations using 3BP-2-derived (HPPAYPPPPVPT) and ABI2-derived (TPPTQKPPSPPMS) ligand peptides. Errors represent the standard error of fitting.

Dissociation constant (μM)			
3BP-2-derived ligand		**ABI2-derived ligand**	
ABL1 SH3	**1.7±0.2**	**ABL1 SH3**	**93±2**
ABL1 SH3$^{pYn/pYc}$	**-**	**ABL1 SH3$^{pYn/pYc}$**	**-**
ABL1 SH3^{YcF}	**3.5±0.3**	**ABL1 SH3^{YcF}**	**116±16**
ABL1 SH3$^{pYn/YcF}$	**>100**	**ABL1 SH3$^{pYn/YcF}$**	**Very weak interaction**
ABL1 SH3^{YnF}	**4.4±0.7**	**ABL1 SH3^{YnF}**	**126±16**
ABL1 SH3$^{YnF/pYc}$	**-**	**ABL1 SH3$^{YnF/pYc}$**	**-**
ABL2 SH3	**2.2±0.2**	**ABL2 SH3**	**158±22**
ABL2 SH3$^{pYn/pYc}$	**-**	**ABL2 SH3$^{pYn/pYc}$**	**-**
ABL2 SH3^{YcF}	**11±2**	**ABL2 SH3^{YcF}**	**186±17**
ABL2 SH3$^{pYn/YcF}$	**>100**	**ABL2 SH3$^{pYn/YcF}$**	**Very weak interaction**
ABL2 SH3^{YnF}	**6.0±0.1**	**ABL2 SH3^{YnF}**	**182±29**
ABL2 SH3$^{YnF/pYc}$	**-**	**ABL2 SH3$^{YnF/pYc}$**	**-**

Table 2. "N"- and "C"-type tyrosine phosphorylation in SH3 domains. ABI1: ABL interactor 1, ABI2: ABL interactor 2, ABL1: Abelson tyrosine-protein kinase 1, ABL2: Abelson tyrosine-protein kinase 2, ARHGAP12: Rho GTPase-activating protein 12, ARHGAP42: Rho GTPase-activating protein 42, BAIAP2L1: Brain-specific angiogenesis inhibitor 1-associated protein 2-like protein 1, BCAR1: Breast cancer anti-estrogen resistance protein 1, BTK: Tyrosine-protein kinase BTK, CRKL: Crk-like protein, CTTN: Src substrate cortactin, DNMBP: Dynamin-binding protein, EPS8: Epidermal growth factor receptor kinase substrate 8, EPS8L2: Epidermal growth factor receptor kinase substrate 8-like protein 2, EPS8L3: Epidermal growth factor receptor kinase substrate 8-like protein 3, FGR: Tyrosine-protein kinase Fgr, FRK: Tyrosine-protein kinase FRK, FYN: Tyrosine-protein kinase Fyn, GRAP2: GRB2-related adapter protein 2, GRB2: Growth factor receptor-bound protein 2, ITK: Tyrosine-protein kinase ITK, ITSN1: Intersectin-1, ITSN2: Intersectin-2, LASP1: LIM and SH3 domain protein 1, LYN: Tyrosine-protein kinase Lyn, MAP3K21: Mitogen-activated protein kinase kinase kinase 21, MAP3K9: Mitogen-activated protein kinase kinase kinase 9, NEDD9: Neural precursor cell expressed developmentally down-regulated protein 9, NOSTRIN: Nitric oxide synthase traffic inducer, PACSIN3: Protein kinase C and casein kinase substrate in neurons protein 3, PIK3R1: Phosphatidylinositol 3-kinase regulatory subunit alpha, PLCG2: Phospholipase C-gamma-2, SASH1: SAM and SH3 domain-containing protein 1, SASH3: SAM and SH3 domain-containing protein 3, SH3GL1: Endophilin-A2, SH3PXD2A: SH3 and PX domain-containing protein 2A, SH3PXD2B: SH3 and PX domain-containing protein 2B, SH3RF1: E3 ubiquitin-protein ligase SH3RF1 /SH3 domain-containing RING finger protein 1, SH3RF3: SH3 domain-containing RING finger protein 3, SORBS2: Sorbin and SH3 domain-containing protein 2, SPTA1: Spectrin alpha chain, erythrocytic 1, SPTAN1: Spectrin alpha chain, non-erythrocytic 1, SRC: Proto-oncogene tyrosine-protein kinase Src, TEC: Tyrosine-protein kinase Tec, TXK: Tyrosine-protein kinase TXK, VAV1: Proto-oncogene vav, VAV3: Guanine nucleotide exchange factor VAV3, YES1: Tyrosine-protein kinase Yes, GEF: Guanine nucleotide exchange factor, HTP: high-throughput, LTP: low-throughput

Protein	Uniprot Identifier	Function	SH3 Domain Position	pTyr Position	Number of HTP Studies	pTyr Type
		pTyrN only				
ABI2	Q9NYB9	Adaptor/Scaffold	451-510	460	5	N
BCAR1	P56945	Docking (Cas scaffolding protein family)	3-65	12	3	N
BTK	Q06187	Tyr kinase (Tec family)	214-274	223	261	N
CRKL	P46109	Adaptor/Scaffold	123-183	132	127	N
EPS8	Q12929	Adaptor/Scaffold	531-590	540	28	N
EPS8L2	Q9H6S3	Adaptor/Scaffold	492-551	501	4	N
EPS8L3	Q8TE67	Adaptor/Scaffold	450-509	459	3	N
FGR	P09769	Tyr kinase (Src family)	77-138	86	10	N
FYN	P06241	Tyr kinase (Src family)	82-143	91	11	N
ITSN1	Q15811	Adaptor/Scaffold	913-971	922	1	N
NEDD9	Q14511	Docking (Cas scaffolding protein family)	3-65	12	4	N
NOSTRIN	Q8IVI9	Adaptor/Scaffold	438-497	447	1	N
PLCG2	P16885	Phospholipase	769-829	778	6	N
SH3GL1	Q99961	Membrane binding	306-365	315	5	N
SH3PXD2B	A1X283	Adaptor/Scaffold	221-280	230	2	N
SH3RF1	Q7Z6J0	Adaptor/Scaffold	134-193	143	1	N
			445-506	454	1	N
SH3RF3	Q8TEJ3	Adaptor/Scaffold	464-525	473	1	N

SPTA1	P02549	Cytoskeleton	977-1036	986	28	N
TXK	P42681	Tyr kinase (Tec family)	82-142	91	2	N
		pTyrC only				
ARHGAP12	Q8IWW6	GTPase activator	12-74	68	1	C
ARHGAP42	A6NI28	GTPase activator	816-874	870	1	C
BAIAP2L1	Q9UHR4	Adaptor/Scaffold	339-402	396	1	C
CTTN	Q14247	Adaptor/Scaffold	492-550	545	22	C
DNMBP	Q6XZF7	Adaptor/Scaffold	1513-1576	1570	1	C
FRK	P42685	Tyr kinase (Src family)	42-110	104	27	C
GRAP2	O75791	Adaptor/Scaffold	271-330	324	7	C
GRB2	P62993	Adaptor/Scaffold	156-215	209	208	C
ITSN1	Q15811	Adaptor/Scaffold, GEF	1074-1138	1132	8	C
			1155-1214	1208	1	C
ITSN2	Q9NZM3	Adaptor/Scaffold, GEF	898-956	950	1	C
LASP1	Q14847	Adaptor/Scaffold	202-261	257	4	C
LYN	P07948	Tyr kinase (Src family)	63-123	117	3	C
MAP3K21	Q5TCX8	Ser/Thr kinase (MAP3K subfamily)	38-102	96	3	C
MAP3K9	P80192	Ser/Thr kinase (MAP3K subfamily)	52-116	110	1	C
PIK3R1	P27986	Adaptor/Scaffold	3-79	73	1	C
SASH1	O94885	Adaptor/Scaffold	557-614	609	1	C
SASH3	O75995	Adaptor/Scaffold	176-232	228	3	C
SH3PXD2A	Q5TCZ1	Adaptor/Scaffold	266-325	319	1	C
SORBS2	O94875	Adaptor/Scaffold	938-999	993	1	C
			863-922	916	3	C
			1041-1100	1096	1	C
		pTyrN and pTyrC				
ABI1	Q8IZP0	Adaptor/Scaffold	446-505	455	8	N
				499	1	C
ABL1	P00519	Tyr kinase (ABL family)	61-121	70	12	N
				115	220	C
ABL2	P42684	Tyr kinase (ABL family)	107-167	116	10	N
				161	219	C
GRB2	P62993	Adaptor/Scaffold	1-58	7	2	N
				52	1	C
ITK	Q08881	Tyr kinase (Tec family)	171-231	180	78	N
				225	2	C
PACSIN3	Q9UKS6	Adaptor/Scaffold	363-424	372	3	N
				418	7	C
SPTAN1	Q13813	Adaptor/Scaffold	967-1026	976	3	N
				1020	13	C
SRC	P12931	Tyr kinase (Src family)	84-145	93	2	N
				139	LTP only	C

TEC	P42680	Tyr kinase (Tec family)	179-239	188	1	N
				233	3	C
VAV1	P15498	Adaptor/Scaffold, GEF	782-842	791	50	N
				836	LTP only	C
VAV3	Q9UKW4	Adaptor/Scaffold, GEF	788-847	797	49	N
				842	1	C
YES1	P07947	Tyr kinase (Src family)	91-152	100	11	N
				146	4	C

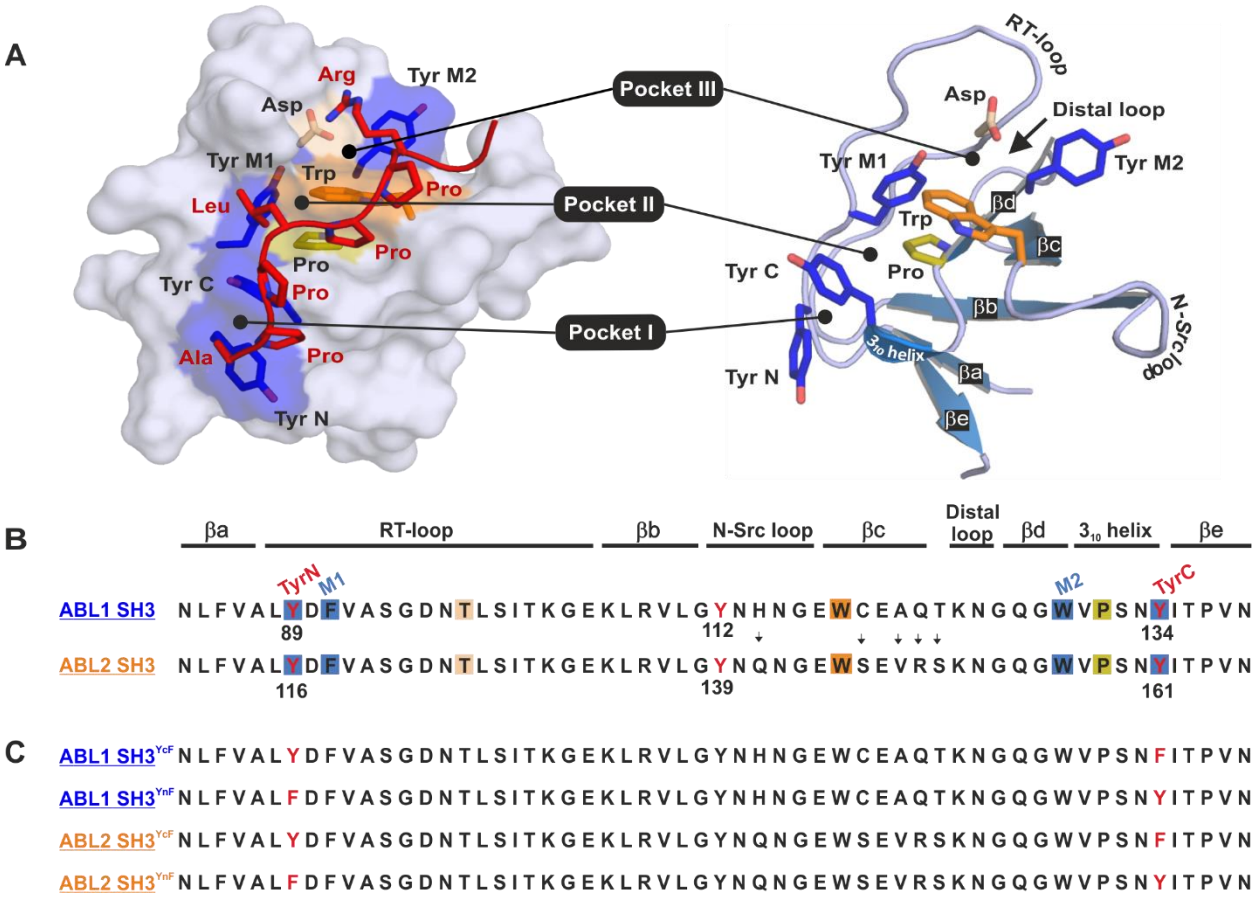

Figure 1. (A) Structure and ligand binding groove of SH3 domains. The SH3 domain of the tyrosine kinase Src in complex with a bound ligand peptide is shown as an example (PDB:1QWE). The ligand binding interface can be divided into three pockets that are mainly flanked by aromatic residues (blue and orange) and a conserved proline (yellow). Binding groove tyrosines starting from the N-terminus are labeled as "N", "M1", "M2", and "C". These positions are referred similarly throughout this work. One or more negatively charged residue of the RT-loop (Asp in Src) orient the ligand (red) by interacting with a positively charged residue on either side of the "PxxP" motif (Arg in this example). (B) Secondary-structural elements and sequence alignment of ABL1 SH3 and ABL2 SH3. Tyrosine phosphorylation sites (based on PhosphoSitePlus) are highlighted in red. Conserved residues of the binding groove are shown with backgrounds corresponding to the color-coding in panel "a". Arrows indicate differences between ABL1 and ABL2. Sequence numbering is based on isoform 1B of both ABL1 (UniProt identifier: P00519-2) and ABL2 (UniProt identifier: P42684-1). Note that in ABL1 SH3 and ABL2 SH3, Phe and Trp residues occupy positions "M1" and "M2", respectively. (C) Protein sequences of Tyr-to-Phe mutant constructs used in this work.

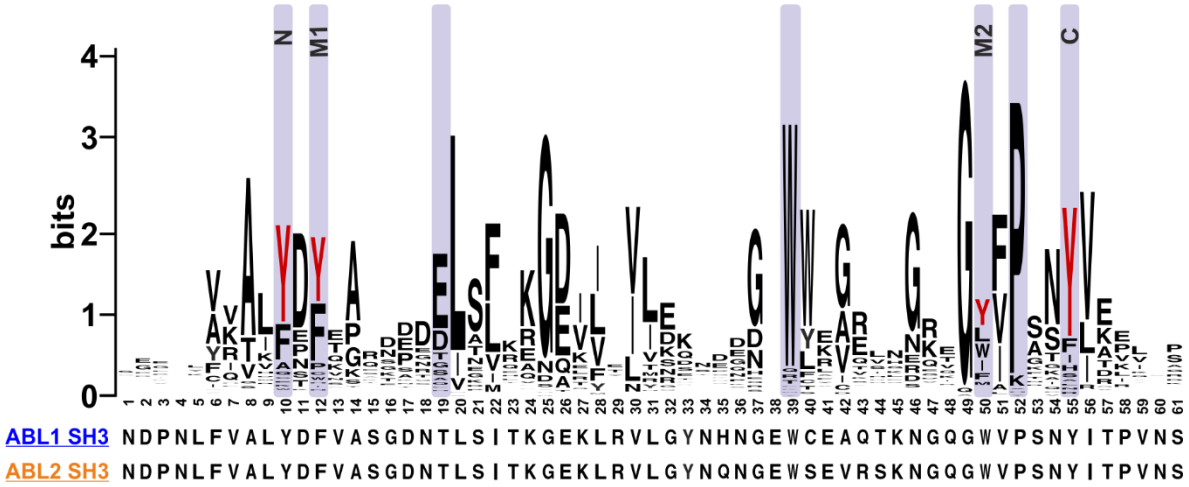

Figure 2. Sequence logo representation of the tyrosine phosphorylated human SH3 domains. Key conserved residues of the ligand binding groove are highlighted in gray background. The four most prominent tyrosine phosphorylation sites (positions 10, 12, 50 and 55, with 32, 13, 20 and 35 occurrences in PhosphoSitePlus, respectively) are indicated in red. (See also the full alignment in Table S2. Note that only positions homologous to ABL1 SH3 are shown here for simplicity.)

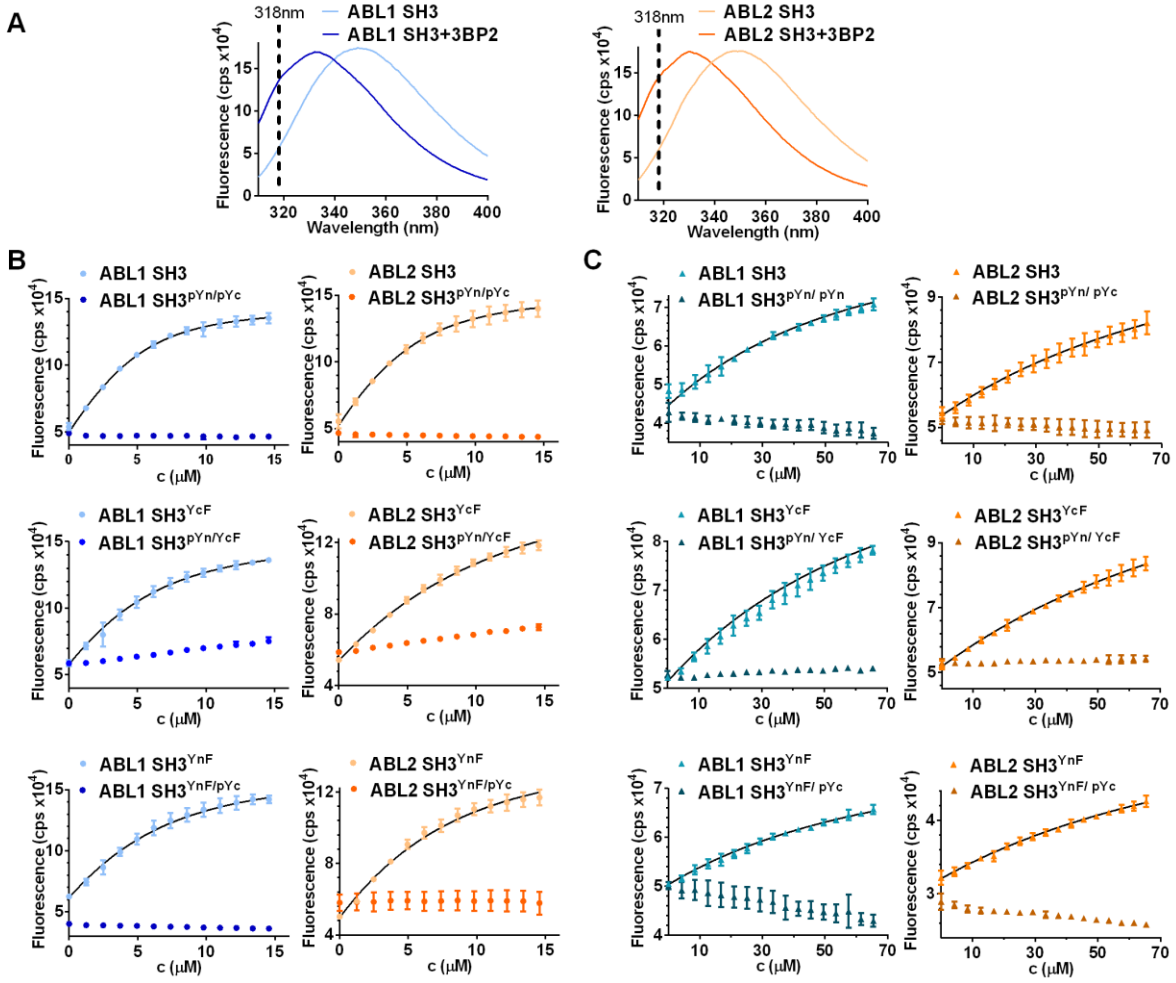

Figure 3. Tryptophan fluorescence-based titrations of ABL1 SH3 and ABL2 SH3. (A) Tryptophan fluorescence emission spectra of free and 3BP-2 peptide-bound ABL1 SH3 and ABL2 SH3. Ligand binding was associated with a remarkable blue shift. The highest intensity difference was observed at 318 nm. (B) Complex formation between ABL1 and ABL2 SH3 variants and 3BP-2 followed by fluorescence intensity changes at 318 nm. Both the doubly-phosphorylated (ABL1 $SH3^{pYn/pYc}$, ABL2 $SH3^{pYn/pYc}$) and Tyr-C-phosphorylated (ABL1 $SH3^{YnF/pYc}$, ABL2 $SH3^{YnF/pYc}$) proteins showed total loss of ligand binding. The inhibitory effect of TyrN phosphorylation (ABL1 $SH3^{pYn/YcF}$, ABL2 $SH3^{pYn/YcF}$) was weaker but still substantial. (C) Complex formation between ABL1 and ABL2 SH3 variants and ABI2 followed by fluorescence intensity changes at 318 nm. Although the ABI2-derived ligand showed much weaker binding compared to 3BP-2 (dissociation constants around 100 μM), the effects of phosphorylation were similar. Error bars represent the standard deviation of three independent measurements.

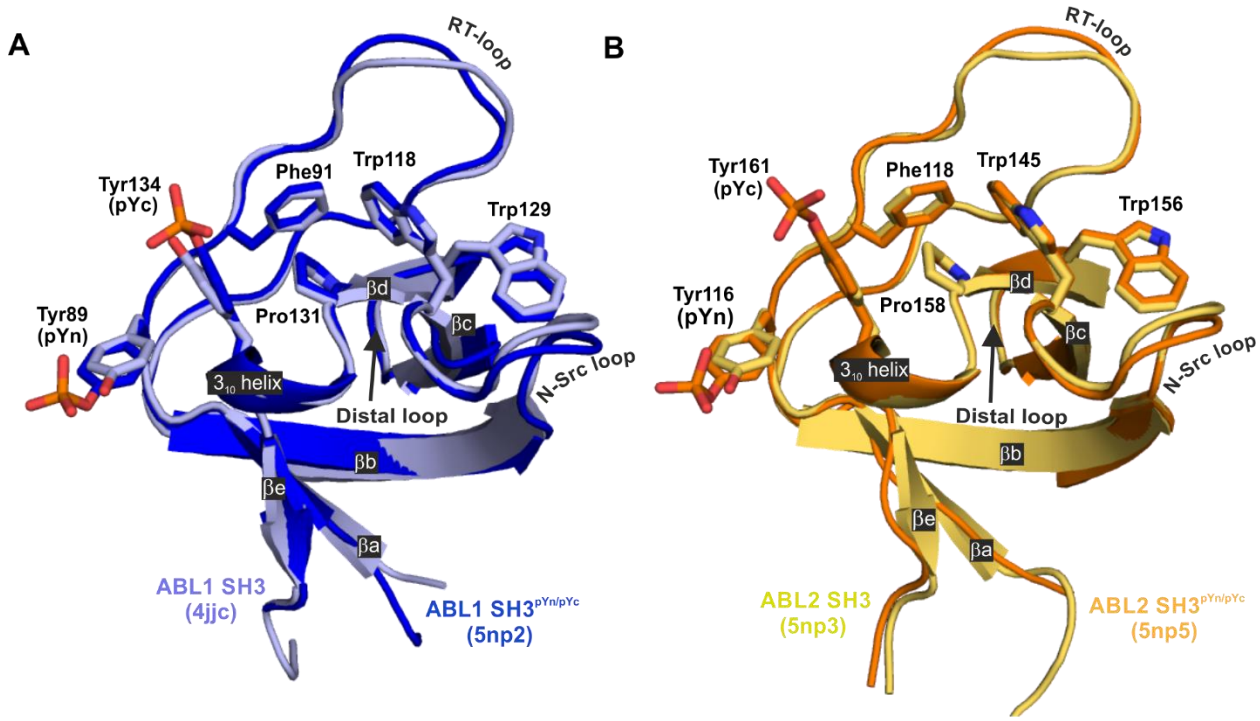

Figure 4. Comparison of the non-phosphorylated and phosphorylated SH3 domains. Structural alignment of (A) ABL1 SH3 (light blue, PDB: 4JJC) with ABL1 $SH3^{pYn/pYc}$ (dark blue, PDB:5np2), (B) ABL2 SH3 (yellow, PDB:5np3) with ABL2 $SH3^{pYn/pYc}$ (orange, PDB:5np5). Key residues of the binding grooves are labeled and shown as sticks.

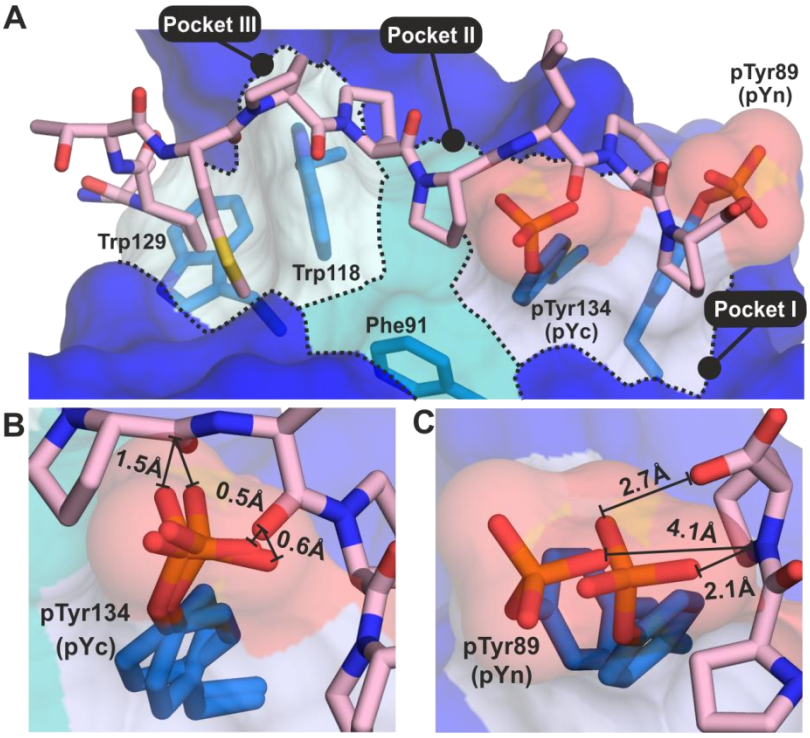

Figure 5. Alignment of the crystal structure of ABL1 SH3$^{pYn/pYc}$ and ABL1 SH3 in complex with a peptide ligand derived from 3BP-1 (PDB: 1ABO(14)). (A) For simplicity, only the ligand (salmon) and the phosphorylated domain are shown. Surfaces of the three neighboring hydrophobic pockets within the binding groove are shown in different colors. (B) The phosphate group of pTyrC (pTyr134) occupies the binding groove making it totally inaccessible for the ligand. (Both Pocket I and Pocket II are affected.). (C) Although the phosphate group of pTyrN (pTyr89) is located at the edge of the binding groove and this sidechain seems to be more flexible, steric clashes with the ligand can be expected. (Mainly Pocket I is affected.)

Structural insights into the tyrosine phosphorylation-mediated inhibition of SH3 domain-ligand interactions

Balázs Mero, László Radnai, Gergo Gógl, Orsolya Toke, Ibolya Leveles, Kitti Koprivanacz, Bálint Szeder, Metta Dülk, Gyöngyi Kudlik, Virág Vas, Anna Cserkaszky, Szabolcs Sipeki, László Nyitray, Beáta G Vértessy and László Buday

J. Biol. Chem. published online January 18, 2019

Access the most updated version of this article at doi: 10.1074/jbc.RA118.004732